JACS
JOURNAL OF THE AMERICAN CHEMICAL SOCIETY
Article
pubs.acs.org/JACS

One Substrate, Five Products: Reactions Catalyzed by the Dihydroneopterin Aldolase from *Mycobacterium tuberculosis*

Clarissa M. Czekster and John S. Blanchard*

Department of Biochemistry, Albert Einstein College of Medicine, 1300 Morris Park Avenue, Bronx, New York 10461, United States

Supporting Information

ABSTRACT: Tetrahydrofolate cofactors are required for one carbon transfer reaction involved in the synthesis of purines, amino acids, and thymidine. Inhibition of tetrahydrofolate biosynthesis is a powerful therapeutic strategy in the treatment of several diseases, and the possibility of using antifolates to inhibit enzymes from *Mycobacterium tuberculosis* has been explored. This work focuses on the study of the first enzyme in tetrahydrofolate biosynthesis that is unique to bacteria, dihydroneopterin aldolase (*Mt*DHNA). This enzyme requires no metals or cofactors and does not form a protein-mediated Schiff base with the substrate, unlike most aldolases. Here, we were able to demonstrate that the reaction catalyzed by *Mt*DHNA generates three different pterin products, one of which is not produced by other wild-type DHNAs. The enzyme−substrate complex partitions 51% in the first turnover to form the aldolase products, 24% to the epimerase product and 25% to the oxygenase products. The aldolase reaction is strongly pH dependent, and apparent pK_a values were obtained for the first time for this class of enzyme. Furthermore, chemistry is rate limiting for the aldolase reaction, and the analysis of solvent kinetic isotope effects in steady-state and pre-steady-state conditions, combined with proton inventory studies, revealed that two protons and a likely solvent contribution are involved in formation and breakage of a common intermediate. This study provides information about the plasticity required from a catalyst that possesses high substrate specificity while being capable of utilizing two distinct epimers with the same efficiency to generate five distinct products.

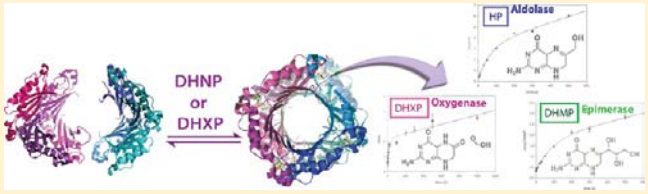

INTRODUCTION

Dihydroneopterin aldolase (DHNA) catalyzes the conversion of 7,8-dihydroneopterin (DHNP) to 6-hydroxymethyl-7,8-dihydropterin (HP) in the biosynthesis of folate, a pathway currently targeted for the treatment of several distinct types of cancers and infections.[1] It has been proposed that DHNA represents a promising new target for the development of antibacterials, underlying the importance of studying the catalytic and chemical mechanism of this enzyme in pathogenic bacteria, such as *Mycobacterium tuberculosis*, the causative agent of tuberculosis.[2,3] DHNAs are interesting enzymes since they catalyze the cleavage of a carbon−carbon bond without the requirement of metals or cofactors, being considered a unique type of aldolase in which a substrate imbedded imine assists in catalysis. In addition to their function as an aldolase, DHNAs catalyze an epimerization reaction in which the configuration of the C2′ carbon−oxygen bond is inverted, forming 7,8-dihydromonapterin (DHMP, Scheme 1).

DHNAs from *Escherichia coli* and *Staphylococcus aureus* (*Ec*DHNA and *Sa*DHNA, respectively) have been characterized, and the reactions catalyzed by these enzymes were shown to possess distinct rate-limiting steps and kinetic parameters. Additionally, mutational studies revealed that acid−base catalysis is probably crucial for the reaction, but pK_a values for group(s) possibly involved in chemistry are lacking.

Here we report the kinetic characterization of the reactions catalyzed by the DHNA from *M. tuberculosis* (*Mt*DHNA) using pH studies, solvent kinetic isotope effects (SKIEs), NMR, and steady-state and pre-steady-state methods and based on our findings conclude that *Mt*DHNA catalyzes three distinct reactions with comparable proficiency. This is the first report of a wild-type DHNA capable of catalyzing a cofactor-independent oxygenase reaction with significant product formation.

Scheme 1. Reactions Catalyzed by *Mt*DHNA

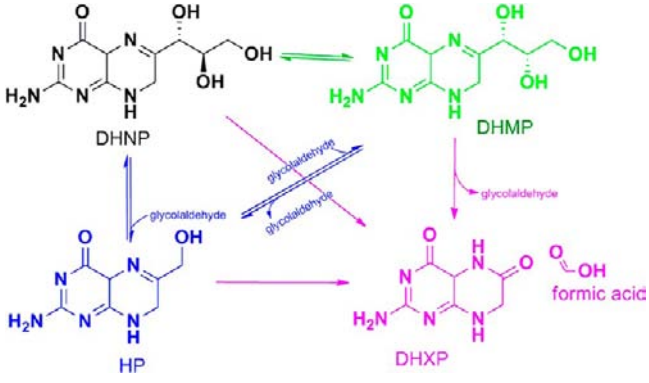

Received: August 22, 2012
Published: November 14, 2012

   dx.doi.org/10.1021/ja308350f | *J. Am. Chem. Soc.* 2012, 134, 19758−19771

MATERIALS AND METHODS

Materials. All chemicals were of analytical or reagent grade and were used without further purification. All pterins were purchased from Schirck laboratories (Jona, Switzerland). Deuterium oxide (99.9 at. % D) was from Cambridge Isotope Laboratories.

Cloning of *Mt*DHNA into Plasmid pET28a(+). The *fol*B gene (*Rv*3607c) encoding DHNA from *M. tuberculosis* was amplified by PCR to generate a PCR product with NdeI and *Hin*dIII restriction sites at the ends. The oligonucleotide primers were 5′- GGAATTC-CATATGGCTGACCGAATCGAAC-3′ and 5′-CCCAAGCTTTCA-TACCGCGCCGCCCGCCG-3′. The amplified DNA product was digested with NdeI and *Hin*dIII, and the purified insert was ligated into pET28a(+) previously linearized with the same restriction enzymes. This recombinant plasmid was transformed into DH5α cells following the instructions supplied by the manufacturer (Invitrogen). Cloning into these restriction sites adds a thrombin-cleavable His6-tag at the N-terminus of the recombinant protein.

Purification of *Mt*DHNA. Competent *E. coli* BL21 (DE3) cells (Novagen) were transformed with the recombinant plasmid pET28a-(+):*folB*, and *Mt*DHNA was expressed and purified as previously described.[4] Protein concentration was determined by using the theoretical extinction coefficient per monomer, accounting for the addition of the sequence MGSSHHHHHHSSGLVPRGSH at the N-terminus of the protein (ε_{280} = 15 470 $M^{-1}cm^{-1}$). The Ni-NTA affinity purified enzyme was dialyzed against 100 mM HEPES containing 50 mM KCl, pH 7.5, and frozen at −80 °C. Protein to be used for sedimentation equilibrium, equilibrium binding, single turnover, and burst experiments was further purified using a gel filtration column (Superdex 200, GE) to make sure that no 7,8-dihydroxanthopterin (DHXP) was bound to the protein after the purification. The apo-*Mt*DHNA generated by this method was less stable and more prone to precipitation at μM concentrations than the DHXP-bound enzyme.

Mass Spectrometry. Purified proteins had their molecular mass determined by LC-ESI-MS. Detailed methods can be found in the Supporting Information.

Ultracentrifugation. Sedimentation equilibrium experiments were conducted at 8000 and 12 000 rpm using six channel centerpieces using an Optima XL-I analytical centrifuge (Beckman). Apo-*Mt*DHNA (25 μM) alone or with equimolar concentrations of neopterin or DHXP were analyzed. The identity of scans taken at 22 and 24 h confirmed that the samples had reached equilibrium. The data were globally analyzed using HeteroAnalysis v1.1.33 (J. L. Cole and J. W. Lary, Analytical Ultracentrifugation Facility, Biotechnology Services Center, University of Connecticut). The best-fit values and joint confidence intervals are reported.

Equilibrium Dissociation Constant. DHXP binding to *Mt*DHNA was measured by fluorescence titration at 25 °C using a Horiba Fluoromax 3 spectrofluorometer (Horiba Jobin Yvon). Excitation and emission wavelengths were 295 and 345 nm, respectively. Titrations were conducted by serial additions of 1 μL aliquots of ligand to a 1 cm^2 quartz cuvette that contained 2 mL of 2 μM of *Mt*DHNA in 100 mM HEPES with 50 mM NaCl, pH 7.0, 1 mM EDTA, 5 mM DTT, and 1% BSA. Fluorescence readings were recorded 2 min after the addition of ligand to allow temperature equilibration, and the dissociation constants were estimated by nonlinear regression using eq 1.[5] A complete description of the equations fitted is available in the Supporting Information. The concentration of DHXP did not exceed 5 μM to avoid inner filter effects.

$$L_b = y_0 + L_t - \frac{2}{3}\cos\left(\frac{\theta}{3}\right)\sqrt{a^2 - 3b} \quad (1)$$

where

$$a = K_{d1} + K_{d2} + S_{1t} + S_{2t} - L_t$$

$$b = K_{d2}{}^*S_{1t} + K_{d1}{}^*S_{2t} + K_{d1}{}^*K_{d2}$$

$$c = -K_{d1}{}^*K_{d2}{}^*L_t$$

$$\theta = \arccos\frac{-2a^3 + 9ab - 27c}{2\sqrt{(a^2 - 3b)^3}}$$

For eq 1, K_{d1} and K_{d2} are the equilibrium binding constants for sites 1 and 2, respectively, S_{1t} and S_{2t} are the total concentrations of sites 1 and 2, L_t is the total ligand (DHXP) concentration, L_b is the concentration of the *Mt*DHNA−DHXP complex, and y_0 is the initial y value.

Fluorescence Steady-State Assays. The aldolase reaction was measured as previously described.[6] Briefly, HP formation was monitored with an excitation wavelength of 430 nm, followed by an increase in fluorescence emission at 535 nm due to HP formation. The slits were 2 and 10 nm for excitation and emission, respectively. The reaction mixture was kept at 25° for 2 min before adding enzyme to ensure that the temperature was equilibrated. After the enzyme was added, there was a lag period of approximately 30 s when DHNP was used as substrate, which was excluded from the fitting to obtain initial rates of reaction. Standard curves for HP fluorescence were measured at all pH values and buffers utilized, and a strong pH dependence of HP fluorescence was observed. Fluorescence emission at 535 nm was plotted as a function of HP concentration, and the slope of this plot was used as a scaling factor to obtain steady-state turnover number, k_{cat}, values for the aldolase reaction. In an attempt to stabilize the enzyme for longer periods of time, 1% BSA was present in all assays, and distinct monovalent and divalent metals were tested, demonstrating no influence on enzyme activity, and thus were excluded from all subsequent assays. Due to the tight binding to DHNP and DHMP and low turnover number, the concentration of *Mt*DHNA was usually between 100−500 nM, comparable to substrate concentrations. Therefore, eq 2 was used to fit initial velocity data, where V_{max} is the maximum velocity, E_0 is the initial total enzyme concentration, S_T is the initial total substrate concentration, K_M is the Michaelis constants for the substrate used.

$$v = V_{max} \times \frac{(E_0 + S_T + K_M) - \sqrt{(E_0 + S_T + K_M)^2 - 4 \times E_0 \times S_T}}{2 \times E_0} \quad (2)$$

NMR-Based Assays. Formation of products in the *Mt*DHNA-catalyzed reaction was followed by ^{1}H NMR. Reactions were performed in 100 mM phosphate, 50 mM NaCl, 1 mM EDTA, 5 mM DTT, 1% BSA, pH 7.0, made containing 90% H_2O and 10% D_2O with 8 mM 4,4-dimethyl-4-silapentane-1-sulfonic acid (DSS) as internal standard. Spectra were collected before enzyme addition, and a control reaction with no *Mt*DHNA was kept at room temperature for 1 h, after which NMR spectra were collected to account for DHNP degradation. NMR spectra were analyzed using MestReNova, using changes in integration values relative to DSS over 1 h. Reactions performed to obtain rates of substrate consumption/product formation had 1 mM DHNP and were initiated with the addition of 3 μM *Mt*DHNA. Reactions to verify complete conversion of DHNP into products had 200 μM DHNP and 10 μM *Mt*DHNA. All spectra were collected in a 14.1 T magnet Bruker DRX600, using a sequence with water suppression. Standard spectra for DHNP, DHMP, DHXP, HP, and 6-formyl-7,8-dihydropterin (F-DHP) were obtained individually.

HPLC Detection of Products. Formation of products in the reverse direction was verified by mixing 200 μM HP and 200 mM glycolaldehyde with 5, 10, 15, or 20 μM *Mt*DHNA. The reaction was stopped after 10 min or 1 h by adding 1 N HCl, followed by neutralization with 1 N NaOH and HPLC analysis. For the formation of products in the forward direction, 220 μM of DHNP or DHMP were mixed with 5, 10, 15, or 20 μM *Mt*DHNA, and reaction was

dx.doi.org/10.1021/ja308350f | J. Am. Chem. Soc. 2012, 134, 19758−19771

stopped after 10 min or 1 h by adding 1 N HCl, followed by neutralization with 1 N NaOH, and HPLC analysis. For all HPLC separations, samples were loaded onto a C_{18} Gemini column (Phenomenex) coupled to a 1100 series HPLC (Agilent), where the mobile phase was 1% methanol and 0.1% acetic acid, pH 3.3 (adjusted with NaOH), the flow rate was 1 mL min^{-1}, and the detection was at 330 nm.

Stopped-Flow Fluorescence Assays. Pre-steady-state experiments were conducted on an Applied Photophysics model SX20 stopped-flow spectrofluorometer equipped with a Xenon lamp, which has a dead time of 3 ms, a 1 cm path length for absorbance measurements, and a 2 mm path length for fluorescence measurements. All experiments were performed at 25 °C in 100 mM HEPES, 50 mM NaCl, 1 mM EDTA, 5 mM DTT, and 1% BSA, and pH 7.0 in water or 90% deuterated water. For the 90% deuterated water experiments, buffers and substrates were prepared in D_2O. For single turnovers in the forward direction using DHNP, 5 and 10 μM *Mt*DHNA were mixed with 1 μM DHNP. For the measurement of SKIEs under single-turnover conditions, 2−5 μM *Mt*DHNA were mixed with 0.5 μM of DHMP in H_2O or 90% D_2O.

For the reverse reaction, 2 μM HP and 5, 11, 23, 34, or 69 μM *Mt*DHNA were mixed. Typically, each observed rate constant was obtained after averaging 3−5 shots and fitting the average to the appropriate exponential equation. The reported concentrations are final, after volumes of 60 μL were mixed from each syringe. Excitation was at 430 nm, and fluorescence emission above 495 nm was detected. Slits were 1 and 2 mm for excitation and emission, respectively.

Stopped-flow traces were fitted analytically using Microsoft Origin version 7, and the first 3 ms of data were discarded when fitting the data. Inspection of residuals provided an assessment of the quality of the fits. The fitting functions had the general form of eq 3, where $y(t)$ is the observed signal at time t, i is the number of transients, A_i is the amplitude of the ith transient, k_i is the observed rate constant for the ith transient, and C is the offset.

$$y(t) = \sum_i A_i e^{-k_i t} + C \tag{3}$$

Quench-Flow Assays. Burst experiments were conducted at 25 °C in a KinTek rapid quench apparatus (model RQF-3) equipped with a constant temperature circulating water bath. For this assay, 33 μM *Mt*DHNA in 100 mM HEPES, 50 mM NaCl, 1 mM EDTA, 5 mM DTT, and 1% BSA, pH 7.0 were mixed with 1 mM DHNP in the same buffer. The reaction was quenched with 1 N HCl, rapidly neutralized with 1 N NaOH, flash frozen to avoid product degradation, and kept at −80 °C until HPLC analysis. A negative control reaction without *Mt*DHNA addition was also collected. Samples were analyzed by HPLC using a C_{18} Gemini column (Phenomenex) and the protocol described above. Standard curves were collected at various concentrations of DHNP, DHMP, DHXP, and HP to obtain integration calibration values. Quenched reactions were thawed immediately before HPLC injection. The curves obtained were fitted to eq 4, which is identical to eq 3 but includes a linear phase, whose rate is represented by v.

$$y(t) = \sum_i A_i e^{-k_i t} + vt + C \tag{4}$$

Oxygen Consumption Assay. Oxygen consumption was measured using a Eutech ECDO6HANDY containing a galvanic dissolved oxygen probe, calibrated with 2 M sodium sulfite. Samples were 5 mL containing 1 mM DHNP, in 100 mM HEPES, pH 7.0 with 50 mM NaCl, 1 mM EDTA, 5 mM DTT, 1% BSA at 25 °C. A control for DHNP degradation was collected before adding enzyme, and the slope of this line was subtracted from the slope obtained in the enzyme-catalyzed reaction to calculate the turnover number. Reactions were started by adding 3 μM *Mt*DHNA.

Coupled Assay with Formate Dehydrogenase. To corroborate that formic acid was formed as one of the products of the oxygenase reaction, 100 μM HP was used as substrate for *Mt*DHNA, and 10 μM formate dehydrogenase from *Candida boidinii* with 1 mM NAD^+ were added to the reaction mixture. The total amount of NADH formed was calculated based on the total change in absorbance at 340 nm using ε_{340} = 6220 M^{-1} cm^{-1}. HPLC assays using methodology described above were used to demonstrate that in the presence of *Mt*DHNA and HP, DHXP was the only product formed.

pH-Rate Profiles. To investigate the role of acid−base catalysis in the *Mt*DHNA-catalyzed aldolase reaction, the pH dependence of the kinetic parameters was determined by measuring initial rates at varying concentrations of DHNP or DHMP. The experiments were conducted throughout the pH range of 4.5−9.5, using the following buffers in a final concentration of 100 mM with 50 mM NaCl, 1 mM EDTA, 5 mM DTT, and 1% BSA: citrate (4.5−5.5), MES (5.5−6.5), HEPES (6.5−8.5), and TAPS (8.5−9.5). The pH stability of the enzyme was tested by incubating the enzyme in the desired buffer for 5 min and conducting the standard assay using HEPES (pH 7.0). pH-Rate profiles with two ionizable groups in the acidic limb and one in the basic limb were fitted to eq 5, where y is the kinetic parameter, C is the pH-independent value of y, H is the proton concentration, K_a is the apparent acid dissociation constant, and K_b is the apparent basic dissociation constant for ionizing groups.

$$\log y = \log\left[\frac{C}{(1 + [H]^2/K_a^2 + K_b/[H])}\right] \tag{5}$$

Steady-State SKIEs for the Aldolase Reaction. SKIEs were measured with the fluorescence assay described above in either H_2O or 93% D_2O, and initial velocities with DHNP or DHMP as substrates were obtained. The reaction was carried out in 100 mM HEPES, 50 mM NaCl, 1 mM EDTA, 5 mM DTT, and 1% BSA, and pH 7.0, a plateau region in the pH-rate profiles to ensure that no pH effects were influencing the SKIEs. Proton inventory studies using DHMP as substrate were conducted at 10% increments of D_2O. Data for the proton inventory on k_{cat}/K_{DHMP} were fitted to eq 6, while data for the k_{cat} proton inventories were fitted to eq 7. For eqs 6 and 7, k_n is the k_{cat} *or* k_{cat}/K_M at each atom % D_2O, k_0 is the k_{cat} or k_{cat}/K_M with H_2O, n is the atom % D_2O, ϕ_1 and ϕ_2 represent transition-state fractionation factors, and $\phi_{solvent}$ represents a fractionation factor arising from solvent contributions.

$$k_n = k_0(1 - n + n\phi_1)(1 - n + n\phi_2) \tag{6}$$

$$k_n = k_0(1 - n + n\phi_1)(1 - n + n\phi_2)(\phi_{solvent}^{\ n}) \tag{7}$$

Global Data Fitting. Fluorescence stopped-flow data with more than one transient phase, and experiments with concentration series, were fit globally by regression analysis based upon numerical integration of the rate equations using KinTek Global Kinetic Explorer version 2.2 (KinTek Corp., Austin, TX). For different ligand concentrations, scaling factors were included in the data fitting process, and estimates for errors on parameters were derived by nonlinear regression and by FitSpace confidence contour analysis.[7,8]

RESULTS AND DISCUSSION

General Properties of the *Mt*DHNA. Purified *Mt*DHNA in the DHXP-bound form and apo-*Mt*DHNA were analyzed by mass spectrometry and sedimentation equilibrium experiments. A total monomeric mass of 16 585 Da was observed by ESI-MS, consistent with the loss of the N-terminal methionine (−131 Da from the predicted molecular weight of 16 716 per monomer, Figure S1). The oligomeric state of purified proteins was determined by sedimentation equilibrium experiments, showing that apo-*Mt*DHNA has a mass consistent with a tetramer (62 299 ± 25 715 Da), while the *Mt*DHNA-NP and *Mt*DHNA-DHXP forms possess the expected mass for octamers (117 853 ± 9774 and 127 525 ± 4105, respectively). Figure S2 shows the data and fits of sedimentation equilibrium experiments. Being both an aldolase and epimerase, DHNA can utilize both DHNP and DHMP as substrates to generate HP. This was confirmed by initial velocity fluorescence assays

dx.doi.org/10.1021/ja308350f | J. Am. Chem. Soc. 2012, 134, 19758−19771

Table 1. Comparison between Kinetic Parameters between Different Reactions and DHNAs from *M. tuberculosis*, *S. aureus*, and *E. coli*

	substrate	k_{cat} (s^{-1})	K_M (μM)	k_{cat}/K_M (M^{-1} s^{-1})
*Mt*DHNA-aldolase	DHNP	0.0054 ± 0.0002	0.165 ± 0.026	$3.6 \times 10^4 \pm 5.5 \times 10^3$
	DHMP	0.0060 ± 0.0002	0.154 ± 0.027	$3.8 \times 10^4 \pm 6.9 \times 10^3$
*Mt*DHNA-epimerase	DHNP	0.0015 ± 0.0003[a]	0.154 ± 0.027	$9.8 \times 10^3 \pm 2.5 \times 10^3$
*Mt*DHNA-oxygenase	DHNP	0.0011 ± 0.0002[a]	0.154 ± 0.027	$7.3 \times 10^3 \pm 1.8 \times 10^3$
*Ec*DHNA[b]	DHNP	0.045	4.6	9.8×10^3
	DHMP	0.01	5.5	1.8×10^3
*Sa*DHNA[b]	DHNP	0.082	7.4	1.1×10^4
	DHMP	0.089	8.0	1.1×10^4

[a]Calculated from linear phase of burst experiments. [b]From ref 9.

monitoring HP formation. Similar K_M values were obtained with both epimers (K_{DHMP} = 150 ± 30 nM, K_{DHNP} = 170 ± 30 nM, Table 1, Figure S3), and the same turnover number was observed (k_{cat} = 0.0060 ± 0.0001 s^{-1}). This low k_{cat} value could not be augmented by the addition of monovalent or divalent metals. Despite its low k_{cat} value, the tight binding interaction with dihydropterin substrates gives *Mt*DHNA a higher k_{cat}/K_M value than other DHNAs.[9] Importantly, the k_{cat}/K_M value obtained for *Mt*DHNA falls within the average of catalytic efficiencies obtained for intermediate metabolism enzymes.[10] It is also important to note that there is a lag of HP formation when DHNP is the substrate, but the lag is absent when DHMP is the substrate. Further information on measured rates can be found in Table S1.

Identification of Products by HPLC. In order to test whether *Mt*DHNA was capable of catalyzing both the epimerase and the aldolase reactions in a reversible manner, reactions were started by adding DHNP, DHMP, or glycolaldehyde and HP. As expected, *Mt*DHNA catalyzes both reactions reversibly, and the reverse reaction has both DHNP and DHMP as products. Surprisingly, a peak with retention time at 8 min, not corresponding to DHNP, DHMP, or HP, was observed in significant amounts, and its formation was directly proportional to the concentration of *Mt*DHNA in the reverse reaction. When the forward reaction is started with either DHNP or DHMP, after 1 h, only this unknown compound was observed as reaction product (Figure 1). This was not caused by degradation of any of the reactants or by contamination in the enzyme preparation. In a recent work conducted with a tyrosine to phenylalanine mutant of *S. aureus* and *E. coli* DHNAs (*Sa*DHNA and *Ec*DHNA, respectively), the wild-type aldolase/epimerase enzyme was converted to an oxygenase whose main product was DHXP, and smaller amounts of F-DHP.[11] Both DHXP and F-DHP were used as HPLC standards, and DHXP had a retention time of 8 min under the same conditions. Additionally, DHXP production was confirmed by LC-MS/MS (data not shown).

Identification of Products by NMR. To further confirm that *Mt*DHNA can produce DHXP as a reaction product, the reaction was monitored by NMR-based assays. Commercial standards of DHNP, DHMP, HP, DHXP, and F-DHP were used for comparison. Conveniently, in the region between 3.9 and 4.3 ppm unique peaks corresponding to each pterin can be observed, allowing the direct observation of each product formed/substrate consumed. Figure 2 shows the time dependence of DHNP consumption, resulting in HP, DHMP, and DHXP formation and that no detectable F-DHP was observed. Conversely, the reverse reaction with glycolaldehyde and HP formed DHNP, DHMP, and DHXP as products (Figure S4).

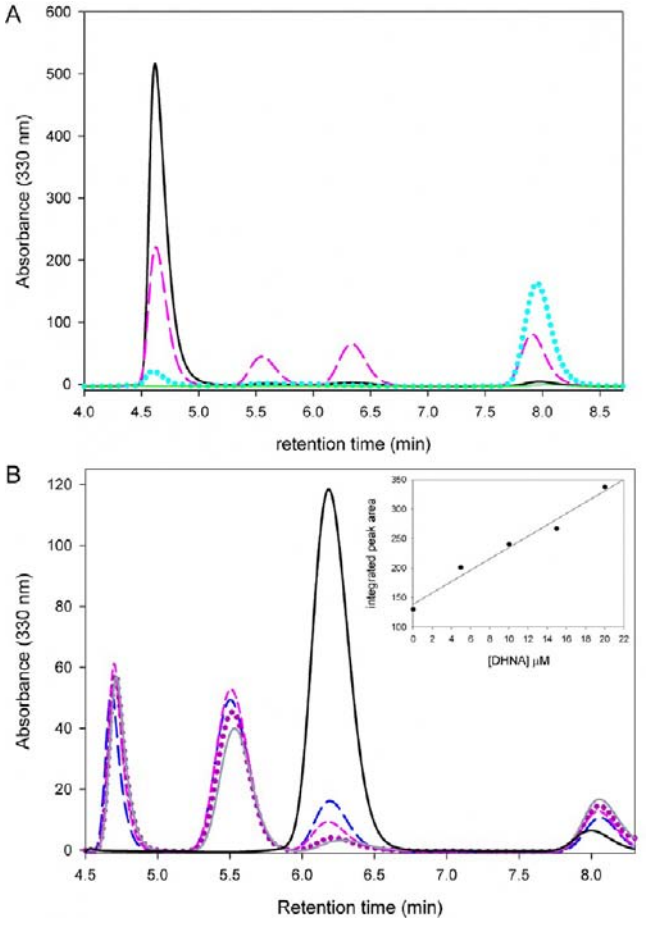

Figure 1. HPLC-based assays showing the forward reaction with DHNP (A) and the reverse aldolase reaction with HP and GA (B). The absorbance of all dihydropterins was observed at 330 nm. (A) Reaction with 10 μM *Mt*DHNA, 220 μM DHNP in 100 mM HEPES pH 7.0 with 50 mM NaCl, 1 mM EDTA, 5 mM DTT: (—, black) curve before adding *Mt*DHNA, (---, pink) after 10 min of reaction, and (..., blue) after 1 h of reaction. (B) Reaction with 10 μM MtDHNA, 220 μM HP, 50 mM GA in 100 mM HEPES pH 7.0 with 50 mM NaCl, 1 mM EDTA, 5 mM DTT: (—, black) curve before adding *Mt*DHNA, (– –, blue) after 10 min of reaction with 5 μM *Mt*DHNA, (---, pink) after 10 min of reaction with 10 μM *Mt*DHNA, (..., purple) after 10 min of reaction with 15 μM *Mt*DHNA, and (—, gray) after 10 min of reaction with 20 μM *Mt*DHNA. The inset represents the replot of the area under the peak with retention time equal to 8.1 min, increasing linearly with the increase in protein concentration. Retention times, in minutes, are 4.7 (DHNP), 5.6 (DHMP), 6.4 (HP), and 8.1 (DHXP).

dx.doi.org/10.1021/ja308350f | J. Am. Chem. Soc. 2012, 134, 19758–19771

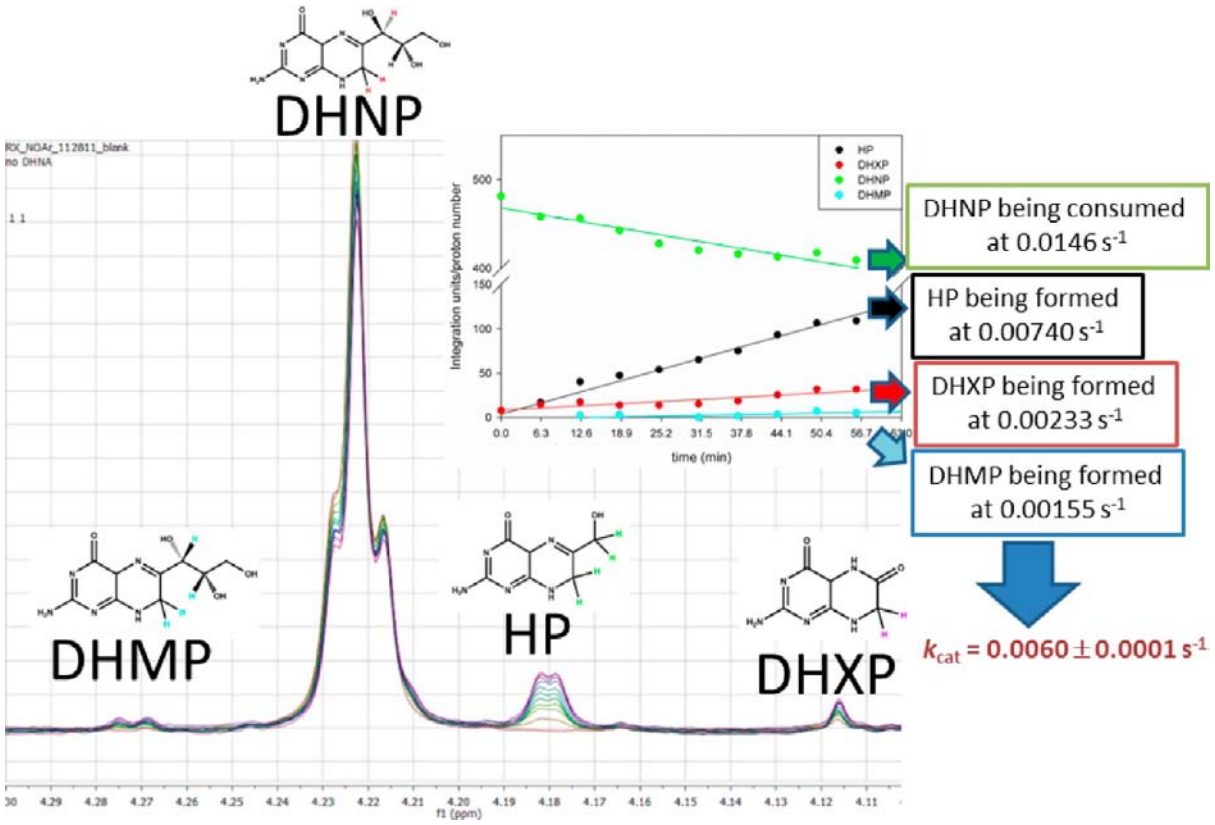

Figure 2. NMR-based assays showing the forward reaction with 1 mM DHNP and 3 μM *Mt*DHNA in 100 mM sodium phosphate pH 7.0 with 5 mM DTT and 1% BSA. The area under the standard DSS was used as reference for the integration of peaks using MestReNova (MestreLab Research S.L.). Values for the integration of each peak corrected for the number of protons of each peak (shown in distinct colors for each molecule) as a function of time are shown in the inset. A negative control without enzyme was kept at 25 °C for 1 h, and this spectrum was subtracted from the ones shown above.

Steady-state rates were obtained for DHNP consumption = 0.015 s^{-1}, HP formation = 0.007 s^{-1}, DHXP formation = 0.002 s^{-1}, and DHMP formation = 0.001 s^{-1}. Importantly, the sum of the steady-state rates of formation of DHMP, HP, and DHXP is comparable to the rate of DHNP depletion. For the reverse reaction, DHMP formation = 0.003 s^{-1}, DHNP formation = 0.013 s^{-1}, and HP consumption = 0.025 s^{-1}, and the rate of DHXP formation could not be determined possibly due to the high concentrations of glycolaldehyde required. Despite faster rates obtained for the reverse reaction as compared to forward reaction, it is important to note that the K_d value for HP is higher than 100 μM and could not be experimentally determined due to inner filter effects and that the K_M value for glycolaldehyde was shown to be in the mM range in DHNAs from other organisms.[12] Finally, NMR-based assays confirmed that when the forward reaction is driven to completion the only product present was DHXP. The current chemical mechanism proposed for mutant DHNAs that form DHXP demonstrates that in order to form DHXP, glycolaldehyde and formic acid will be the other products (Scheme 2). Similar reactions catalyzed by other cofactor and metal-independent oxygenases have been characterized and are believed to be irreversible.[13] Thus, despite the fact that HP formation over DHXP is kinetically favored, irreversible formation of DHXP would slowly result in its accumulation so that DHXP would build up until it is the only product present in the reaction mixture.

DHXP Binding to MtDHNA. To further investigate the interaction between *Mt*DHNA and DHXP, equilibrium binding experiments were performed, demonstrating that DHXP binds tightly to *Mt*DHNA Figure 3. Purified *Mt*DHNA has an absorption maxima at 310 nm, indicating that the enzyme copurified with bound DHXP. DHXP could be removed by gel filtration, but the apoprotein was unstable and prone to precipitation. The apoprotein was utilized for equilibrium binding experiments. Attempts to fit the data to a one site binding quadratic equation yielded a fitted curve that diverges considerably from experimental data, and better fits were obtained when using a hyperbolic equation for a two site binding interaction. Knowing that an equation accounting for ligand depletion was necessary since the concentrations of free DHXP were not equal to the total concentration of DHXP in the assay, an equation proposed by Wang et al. which considers two binding sites and ligand depletion was used (eq 1).[5,14] Approximate equilibrium dissociation constants were obtained for the two sites, being K_{d1} = 0.07 ± 0.07 and K_{d2} = 6 ± 4 μM. Despite the high standard errors, this is the most realistic model to be fitted. It is possible that, because protein fluorescence was monitored, the contribution for fluorescence emission for the initial binding site is not the same as the one for the subsequent binding site, a situation not anticipated using this equation. Nevertheless, this fitting allowed an estimate of the affinity of DHXP binding, and the values of K_{d1} and K_{d2} indicate negative cooperativity (Figure S5). The advantages of negative cooperativity have been extensively discussed for several enzymatic reactions, and calculations suggest that enzymes that exhibit such behavior respond less sensitively to broader ranges of metabolite concentrations.[15] Also, it was previously

dx.doi.org/10.1021/ja308350f | *J. Am. Chem. Soc.* 2012, 134, 19758−19771

Scheme 2. Proposed Chemical Mechanism for Aldolase, Epimerase, and Oxygenase[a]

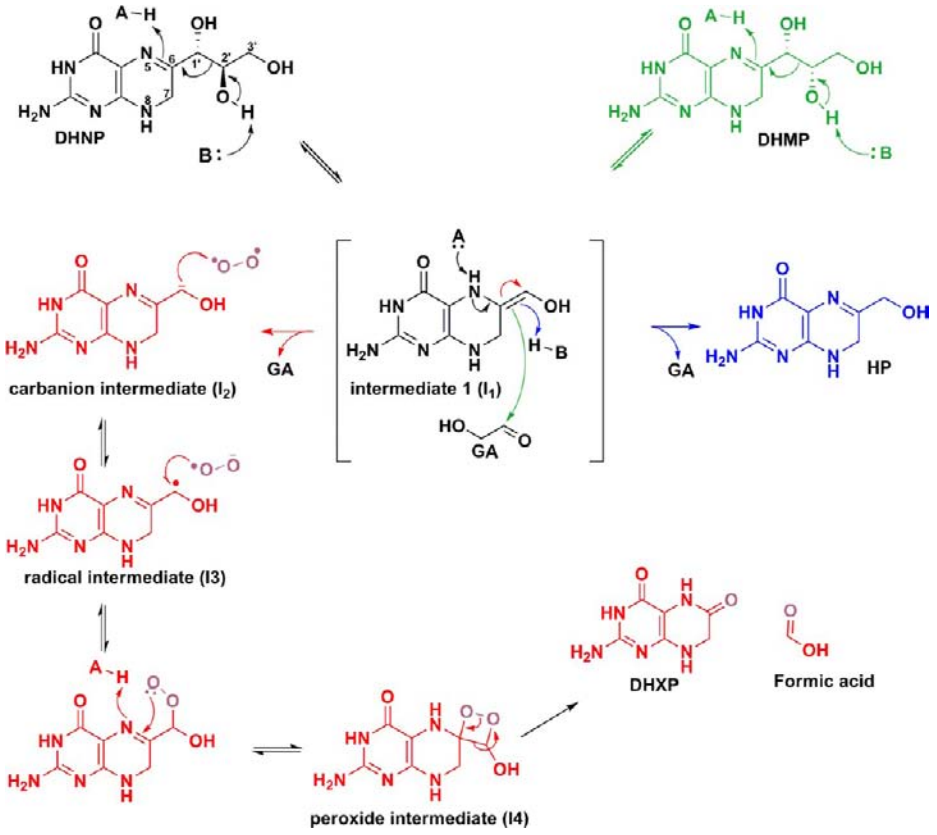

[a]Intermediate 1 (I1) has three possible fates, represented by green, blue, and red arrow. I1 partitions to form the epimerase (green arrow, attack on GA's carbonyl forms DHMP), aldolase (blue arrow, abstraction of a proton from conjugated acid forms HP) or oxygenase (red arrow, formation of a carbanion intermediate which reacts with oxygen generates DHXP) reaction products.[11].

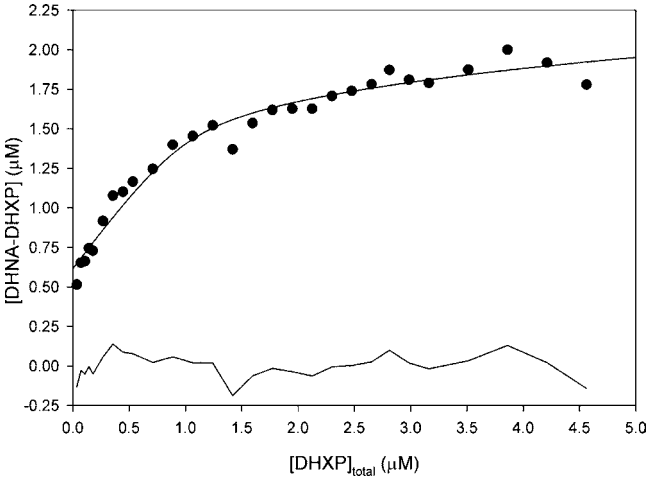

Figure 3. DHXP binding to *Mt*DHNA measured by fluorescence titration. Excitation and emission wavelengths were 295 and 345 nm, respectively. Serial additions of 1 μL aliquots of ligand were made to a 1 cm^2 quartz cuvette that contained 2 mL of 2 μM of *Mt*DHNA in 100 mM HEPES with 50 mM NaCl, pH 7.0, 1 mM EDTA, 5 mM DTT, and 1% BSA. Dissociation constants were estimated by nonlinear regression using eq 1, giving K_{d1} = 0.07 ± 0.07 and K_{d2} = 6 ± 4 μM. More details about other equations fitted are available in the Supporting Information. The line in the bottom of the graph represents the residuals of the fit.

shown that DHNP was an activator of DHNA, inducing octamer formation.[16] It might be advantageous for this particular enzyme to be regulated by distinct mechanisms depending on which metabolite is present, since DHNP is a potent antioxidant present at μM concentrations in sites of inflammation and free-radical damage.[17−19]

Pre-Steady-State Burst. To verify whether the *Mt*DHNA-DHNP complex is capable of partitioning to generate the aldolase, epimerase, and oxygenase products in the first turnover, burst experiments were performed using a quench-flow apparatus. Figure 4 shows that in the first turnover, DHNP is consumed at 0.018 s^{-1} to form HP (0.037 s^{-1}), DHMP (0.009 s^{-1}), and DHXP (0.065 s^{-1}). Analysis of the burst amplitude reveals that 51% of the *Mt*DHNA-DHNP complex is turned over to generate HP, 24% generates DHMP, and the other 25% produces DHXP. The rates for the linear phases of each of the reactions correlate well with the steady-state rates measured by NMR-based assays, demonstrating that in spite of the small k_{cat} values for all three reactions, each can be independently and reproducibly determined. The oxygenase reaction has the fastest burst rate, but production of DHXP generates a stable octameric *Mt*DHNA-DHXP complex (discussed above) that represents an inactive complex. In order to proceed to the next productive turnover, DHNP or DHMP need to compete for the pterin binding site, displacing DHXP. It is important to point out that in other DHNAs previously characterized, the aldolase reaction is by far the most significant to be catalyzed, and even though *Ec*DHNA shows significant epimerase activity while *Sa*DHNA shows almost none, neither of these wild-type enzymes produced DHXP in a

dx.doi.org/10.1021/ja308350f | J. Am. Chem. Soc. 2012, 134, 19758−19771

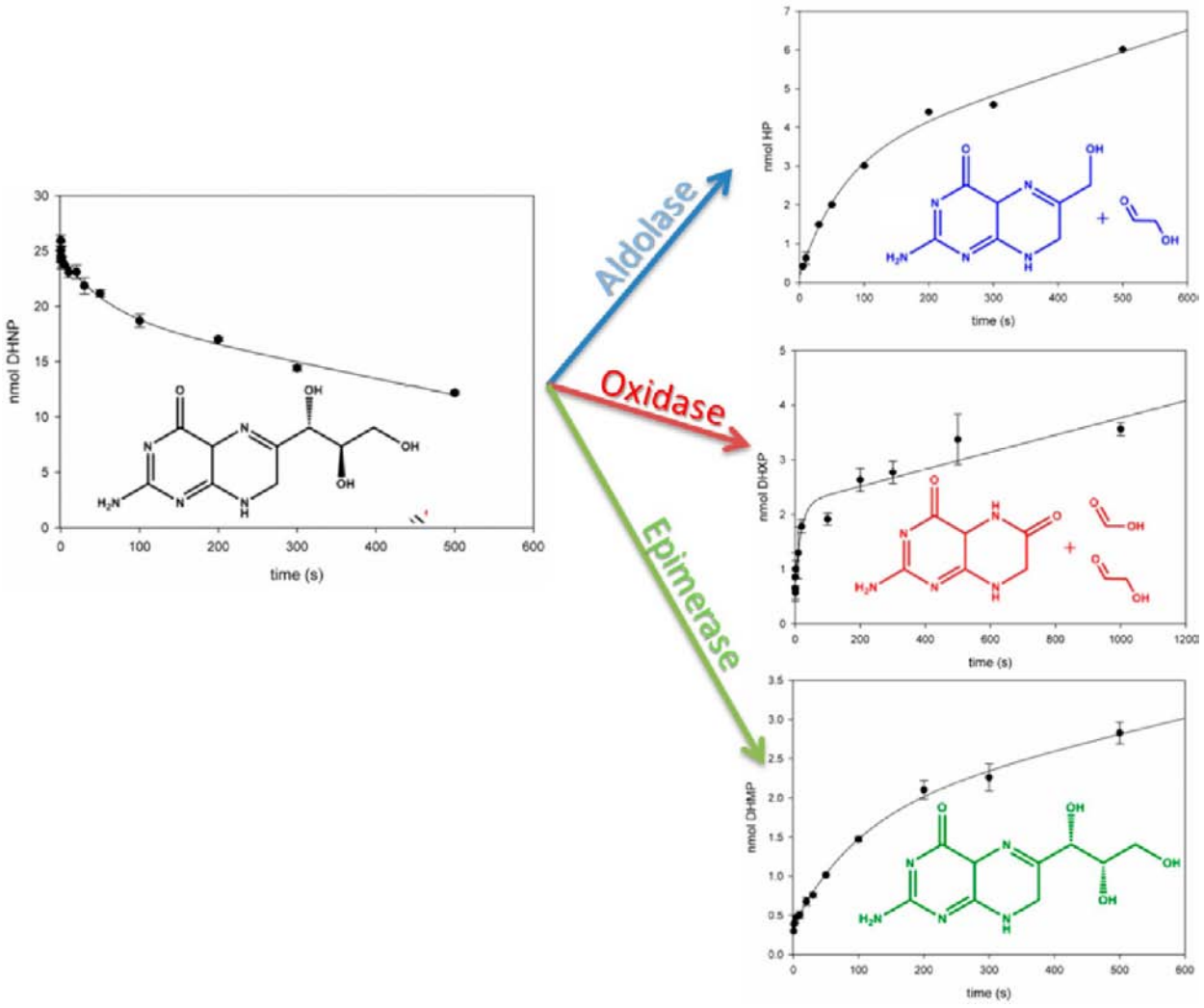

Figure 4. Multiple turnover showing bursts of substrate consumption and in the formation of the three dihydropterin products; 33 μM *Mt*DHNA was mixed with 1 mM DHNP in 100 mM HEPES, pH 7.0, with 50 mM NaCl, 1 mM EDTA, 5 mM DTT, 1% BSA, and the reaction was quenched at different time points with 1N HCl, neutralized with 1N NaOH, and flash frozen for posterior HPLC analysis. Standard curves with DHNP, DHMP, HP, and DHXP were used as standards for concentration. The values obtained were: DHNA consumption $k_{\text{burst-DHNP}}$ = 0.018 ± 0.006 s^{-1} and $k_{\text{cat-DHNP}}$ = 0.011 ± 0.008 s^{-1}; HP formation $k_{\text{burst-HP}}$ = 0.037 ± 0.031 s^{-1} and $k_{\text{cat-HP}}$ = 0.009 ± 0.001 s^{-1}; DHMP formation $k_{\text{burst-DHMP}}$ = 0.010 ± 0.003 s^{-1}, $k_{\text{cat-DHMP}}$ = 0.0015 ± 0.0006 s^{-1}; and DHXP formation at $k_{\text{burst-DHXP}}$ = 0.07 ± 0.03 s^{-1}, $k_{\text{cat-DHXP}}$ = 0.0011 ± 0.0002 s^{-1}. Based on the burst amplitudes (total product formation = 6.0 nmol), the partition to form each product can be calculated so that 51% of the *Mt*DHNA-DHNP partitions form HP, 24% form DHMP, and 25% form DHXP.

significant manner (<2% DHXP produced in comparison to the epimerase and aldolase products).[12]

Oxygen Consumption Assay. To test whether the oxygen source for the oxygenase reaction generating DHXP was dissolved oxygen, an oxygen consumption assay was conducted. Figure 5 compares the decrease in dissolved oxygen concentration before and after adding *Mt*DHNA. Stability studies with reduced pterins demonstrated that dihydro and tetrahydropterins slowly react with dissolved oxygen to generate oxidized pterins and that DHXP is the major oxidation product of DHNP, 7,8-dihydrobiopterin, and 7,8-dihydrofolic acid.[20] This spontaneous reaction is very slow ($t_{1/2}$ = 60 h) and significantly slower than the *Mt*DHNA-catalyzed oxidation. Importantly, the corrected rate of oxygen consumption (0.0025 s^{-1}) is equal, within experimental error, to the rate of DHXP formation determined by NMR-based assays (0.0023 s^{-1}), further indicating that in order to produce DHXP, dissolved oxygen is consumed. Both mutant *Sa*DHNA and *Ec*DHNA that were converted in oxygenases upon a tyrosine to phenylalanine substitution (Y54F and Y53F, respectively) consumed dissolved oxygen to convert DHNP into DHXP.[11]

Formation of Formic Acid. Formation of formic acid as one of the reaction products was probed using a coupled assay with formate dehydrogenase. When 100 μM HP was used as substrate for the oxygenase reaction, the formation of 80 μM NADH occurred. Knowing that every molecule of formic acid consumed is associated with the formation of one molecule of NADH, under the experimental conditions tested the majority of HP was converted in DHXP (Figure S6). It is possible that the combined $\Delta\varepsilon_{340}$ is smaller than the ε_{340} for NADH alone, since HP and DHXP have some residual absorbance at 340. The conversion of HP to DHXP in the presence of *Mt*DHNA was confirmed by HPLC (Figure S7).

pH-Rate Profiles. DHNAs are cofactor and metal independent, relying solely on acid−base catalysis to catalyze the cleavage of a carbon−carbon bond.[21] Despite the

dx.doi.org/10.1021/ja308350f | J. Am. Chem. Soc. 2012, 134, 19758−19771

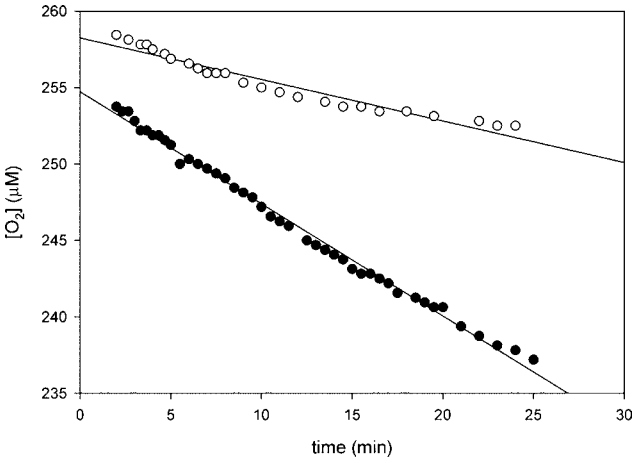

Figure 5. Oxygen consumption assay. The reaction was conducted with 1 mM DHNP in 100 mM HEPES, pH 7.0, with 50 mM NaCl, 1 mM EDTA, 5 mM DTT, and 1% BSA. (○) Reaction mixture without enzyme and (●) reaction mixture after the addition of 3 μM *Mt*DHNA. The slope of the curve without enzyme was subtracted from the one were *Mt*DHNA was added, yielding a k_{cat} of 0.0025 s^{-1}.

availability of structural and kinetic information, pH studies are still lacking for all DHNAs characterized to date. We investigated the influence of pH on binding and catalysis of the aldolase reaction, using DHNP or DHMP as substrates. In these studies, two kinetic parameters were evaluated: k_{cat}/K_M, which reports on steps from free enzyme and free substrates up to and including the first irreversible step, in this case glycolaldehyde release, and k_{cat}, which includes all steps from the formation of a productive enzyme−substrate complex until the release of the last product. Identical patterns were obtained for both epimers: For the k_{cat}/K_M profile, an apparent pK_a of ∼6.0 was assigned to two groups required to be unprotonated, and an apparent pK_a of 7.4 was assigned to one group required to be protonated. No pH dependence was observed for either k_{cat} profile, indicating that a pH-independent process is limiting enzyme turnover (Figure 6). The pH independence of k_{cat}, while there is a strong pH dependence for k_{cat}/K_M, could also indicate that substrate binding can only occur to the correctly protonated form of the enzyme. Due to the fact that SKIEs under steady-state conditions (see below) presented considerably higher values in $^{D_2O}k_{cat}/K_M$ than in $^{D_2O}k_{cat}$, we believe the latter to be less likely than the presence of a pH-independent process limiting turnover, which would increase reverse commitments and decrease the magnitude of the $^{D_2O}k_{cat}$.

Mutational and structural studies conducted with the *Sa*DHNA and *Ec*DHNA showed that five residues in the active site could be playing catalytic roles. All these residues are conserved in DHNAs, including *Mt*DHNA. For the *Sa*DHNA and *Ec*DHNA, mutations of E22, E74, and K99 (*Mt*DHNA numbering) decreased k_{cat}/K_M for both pterin epimers by 3, 2, and 4 orders of magnitude, respectively.[9] Interestingly, mutation of Y54 to a phenylalanine converted *Sa*DHNA and *Ec*DHNA into oxygenases whose main reaction product was DHXP.[11] This residue is also conserved throughout species, being at the monomer−monomer interface such that Y54 from subunit 1 interacts with the active site of subunit 2, whose Y54 interacts with the active site of subunit 3, and so on. The role of Y54, although important, remains a subject of debate. It could be acting as a catalytic acid to protonate intermediate 1 (I1), or it could be modulating water accessibility to the active site, required to protonate N5. Based on the p*K* values reported here, another possibility is that proximity of Y54 to K99 lowers the pK_a of the general base, which facilitates deprotonation and neutralization, avoiding charge repulsion.[22] pK_a values significantly lower than expected for primary amines were observed for a lysine acting as a general acid in the reaction catalyzed by acetoacetate decarboxylase, in which proximity to another lysine residue was shown to decrease the pK_a values of both groups.[23]

Furthermore, the chemical mechanism proposed for the Y54F mutants indicates the formation of a carbanion intermediate (I2), which reacts with dioxygen to form DHXP as reaction product (Scheme 2). This type of mechanism seems to be common for cofactor-independent dioxygenases; an initial proton abstraction that generates a carbanion intermediate, which then reacts with dioxygen. Additionally, several examples of enzymes that produce carbanionic intermediates and possess oxygenase side reactions are known, and it has been hypothesized that cofactor-independent oxygenases could be utilizing the reactivity of carbanions with electrophiles as a general catalytic strategy.[13,24] As illustrated in Scheme 2, I1 has three possible fates: π electrons from the C6−C1′ double bond can abstract a proton from the conjugate acid of the general base (K99 in the Figure S8) to generate HP (blue arrow) or attack the carbonyl group of glycolaldehyde to form DHMP. Finally, deprotonation of N5 can generate the C1′ carbanion (I2), and after the formation of the three intermediates shown, generate DHXP and formic acid.[11] The rate-limiting nature of the proton abstraction from the conjugate acid could be influencing the formation and stabilization of the carbanion intermediate and its reaction with dioxygen.

Single Turnover Studies on the Reverse Aldolase Reaction. To evaluate the internal reversibility of the aldolase reaction, single turnover experiments were performed using 2 μM HP, 50 mM glycolaldehyde, and increasing concentrations of *Mt*DHNA monitoring decrease in fluorescence emission above 495 nm due to HP disappearance. The observed rate constant for HP consumption showed a linear dependence with increasing enzyme concentration, further demonstrating the low affinity of HP for *Mt*DHNA. Because binding was considerably rate limiting, thus contributing to the observed rate constant obtained under single turnover conditions, pseudofirst-order conditions were not satisfied, complicating the analysis by analytical fitting (Figure S9). In order to obtain estimates for the rates of HP binding and the rate of the reverse chemical step, data were analyzed by numerical integration using KinTek Global Explorer. A simple two step model was utilized (Scheme 4). Based on the boundaries obtained for k_1 and k_{-1} (k_1 between 0.07 and 0.17 μM^{-1} s^{-1}, k_{-1} between 5.2 and 19.3 s^{-1}), a K_d between 30 and 250 μM can be estimated. Based on the fact that no saturation was observed in equilibrium binding experiments with up to 100 μM HP (data not shown), the true K_d value is more likely to approximate the upper boundary. It is important to point out that *Mt*DHNA binds DHNP, DHMP, and DHXP very tightly but possesses considerably lower affinity for HP, the pterin product of the aldolase reaction, a discrimination absent in previously characterized DHNAs in which binding of HP, DHNP, and DHMP occurs with comparable affinity. The best-fitted apparent value for the reverse chemical step was 0.52 s^{-1} (k_2 boundaries: 0.31−0.81). The value for k_{-2} was kept fixed at 0.037 s^{-1}, based on the value obtained in quench-flow burst experiments for the conversion of *Mt*DHNA-DHNP to

dx.doi.org/10.1021/ja308350f | J. Am. Chem. Soc. 2012, 134, 19758−19771

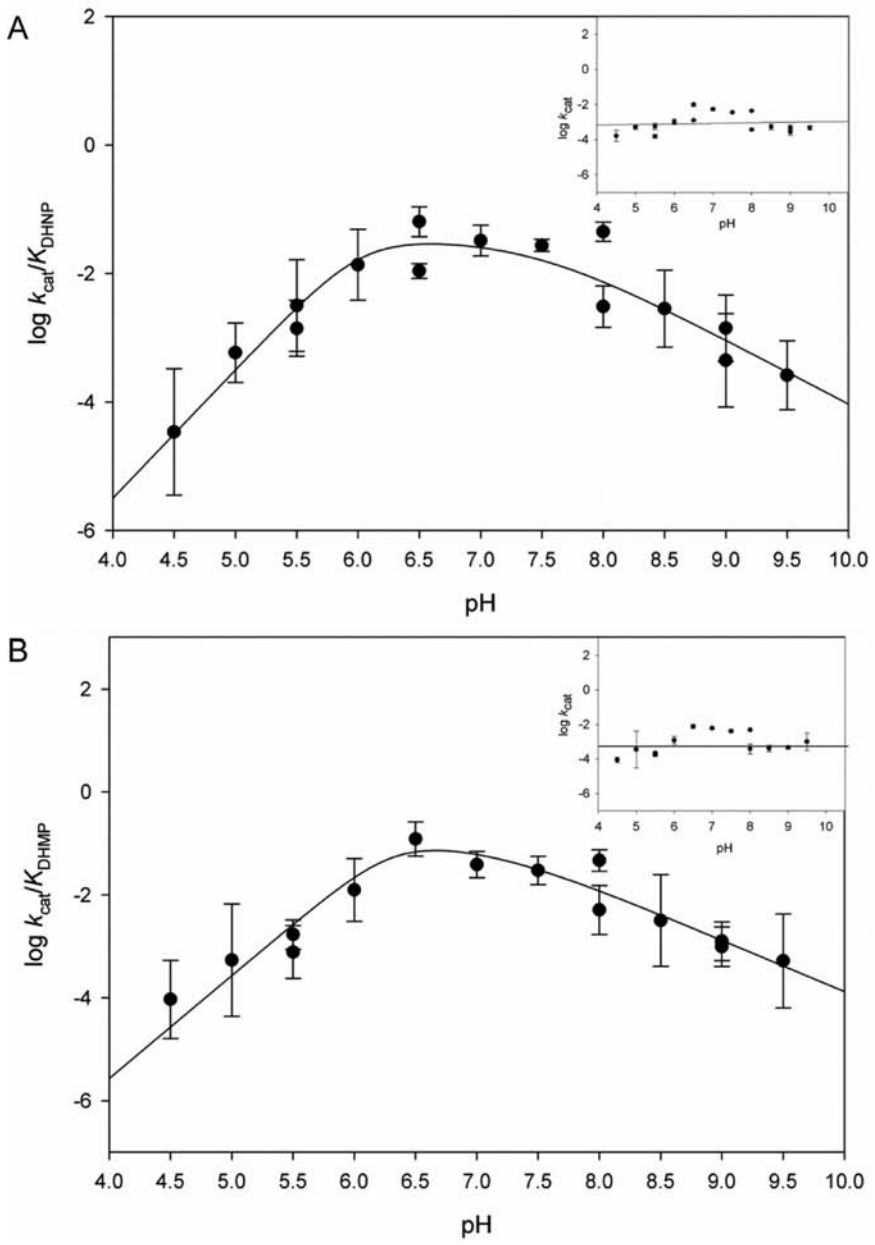

Figure 6. pH Dependence of (A) log k_{cat}/K_{DHNP} and log $k_{cat\text{-}DHNP}$ (inset) and (B) log k_{cat}/K_{DHMP} and log $k_{cat\text{-}DHMP}$ (inset). The lines represent fits to eq 7. The values obtained were 6.0 ± 0.5 with slope of two in the acidic limb and 7.4 ± 0.3 with a slope of one in the basic region (A) and 6.1 ± 0.3 with slope of two in the acidic limb and 7.1 ± 0.3 with a slope of one in the basic region (B). The following buffers were utilized with 50 mM NaCl, 1 mM EDTA, and 5 mM DTT: 100 mM citrate (pH 4.5–5.5), 100 mM MES (5.5–6.5), 100 mM HEPES (6.5–8.0), 100 mM TAPS (8.0–9.0), 100 mM CHES (9.0–9.5). Calibration curves for HP fluorescence emission at 535 nm were obtained for all buffers utilized. Lines are fits to eq 5.

Scheme 4

*Mt*DHNA-HP-glycolaldehyde. Interestingly, the on-enzyme reverse reaction is considerably faster than the forward reaction, but it probably rarely occurs since HP and glycolaldehyde bind extremely weakly. In the *Sa*DHNA-catalyzed reaction, the rate of conversion of *Sa*DHNA-HP-glycolaldehyde into I1 is very fast (100 s^{-1}) if compared to the rates of conversion of both *Sa*DHNA-DHNP and *Sa*DHNA-DHMP into I1 (0.33 and 0.076 s^{-1}, respectively).

Steady-State SKIEs for the Aldolase Reaction. In order to investigate the rate-limiting nature of protonation steps, SKIEs and proton inventory studies were conducted for the aldolase reaction using DHNP or DHMP as substrates. When DHNP was the substrate, $^{D_2O}k_{cat\text{-}DHNP}$ = 1.2 ± 0.1 and $^{D_2O}k_{cat}/K_{DHNP}$ = 2.6 ± 0.6 were obtained, while when DHMP was used as substrate, values were $^{D_2O}k_{cat\text{-}DHMP}$ = 1.6 ± 0.1 and $^{D_2O}k_{cat}/K_{DHMP}$ = 4.1 ± 0.9 (Figure 7A,B, respectively). The difference in SKIE values when using distinct epimers can be explained based on the different orientation of the C2′-hydroxyl group, from which proton abstraction occurs. Based on the crystal structures of *Sa*DHNA with bound substrate analogs monapterin (MP) and neopterin (NP) (Figure S8), it has been suggested that the complex *Sa*DHNA–MP adopts an

dx.doi.org/10.1021/ja308350f | *J. Am. Chem. Soc.* 2012, 134, 19758–19771

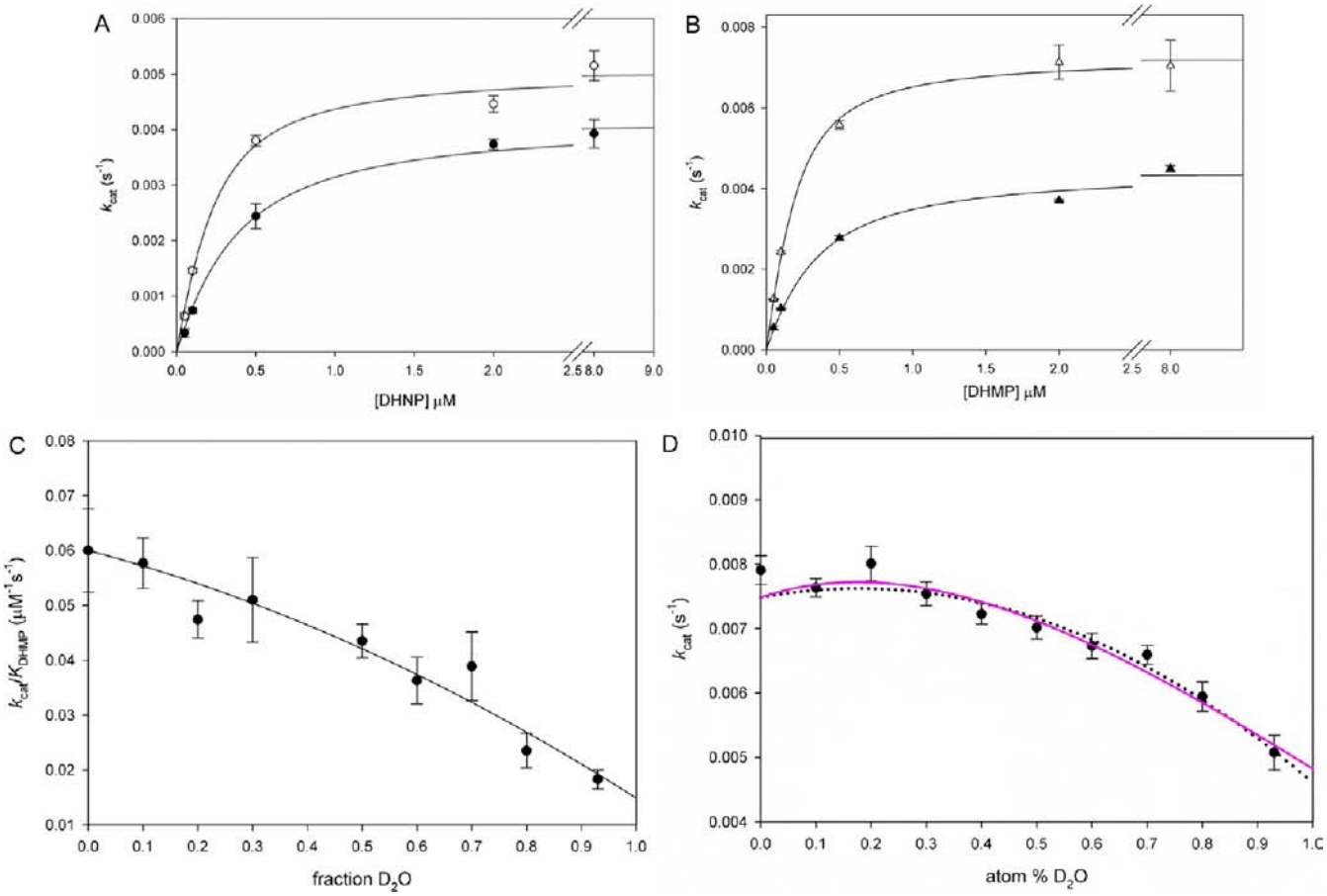

Figure 7. SKIEs with (A) DHNP or (B) DHMP. The lines represent fit to eq 2. The values obtained for k_{cat} or k_{cat}/K_M in H_2O were divided by the ones obtained at 93% fraction of D_2O. The reaction was carried out in 100 mM HEPES, 50 mM NaCl, 1 mM EDTA, 5 mM DTT, and 1% BSA, pH 7.0, a plateau region in the pH-rate profiles to ensure that no pH effects were influencing the SKIEs, and the pH value was not altered by increasing fractions of D_2O. (C,D) Proton inventory using DHMP as substrate. The fitted line in (C) is a fit to eq 7, indicating the contribution of two transition-state protons, one with a normal fractionation factor (ϕ) and one with an inverse fractionation factor. The calculated $^{D_2O}k_{cat}/K_{DHMP}$ using the relationship $^{D_2O}k_{cat}/K_{DHMP} = (1/\phi_{TS1})(1/\phi_{TS2})$ was equal to 4.0 (where $\phi_{TS1\ and}\ \phi_{TS2}$ are the fractionation factors for transition-state protons 1 and 2). The continuous line in (D) is a fit to eq 6, while the dotted line represents a fit to eq 7, indicating the contribution of two transition-state protons with an inverse and a normal fractionation factor each, yielding a normal isotope effect, and various solvent protons contributing with inverse isotope effects. For all data points, the values obtained for k_{cat} or k_{cat}/K_M in H_2O were divided by the ones obtained at different fractions of D_2O, and the errors were propagated as described elsewhere.[32]

unfavorable orientation, and proton abstraction from the C2′-bound hydroxyl group requires the breakage of two hydrogen bonds and a 180° rotation to align the C2′−OH from MP with the catalytic lysine and for catalysis to occur (K99 in *Mt*DHNA).[25] The SKIEs determined here corroborate this hypothesis, since the $^{D_2O}k_{cat}/K_{DHMP}$ is two times larger than $^{D_2O}k_{cat}//K_{DHMP}$, and $^{D_2O}k_{cat\text{-}DHMP}$, despite being small, is significant and larger than $^{D_2O}k_{cat\text{-}DHNP}$.

Because higher observed SKIE values were obtained when DHMP was the substrate, proton inventory studies using DHMP were carried out to obtain more information about the number of protons originating the observed SKIE. In the proton inventory on V/K_{DHMP}, a better fit of the data was obtained with a model predicting contributions from two transition-state protons than to a linear dependence (one transition-state proton) model (further discussion about proton inventory data fitting is available in Table S2 in the Supporting Information). With this model, fractionation factors of 1.38 ± 0.23, and 0.18 ± 0.07 were obtained, yielding a calculated SKIE of 4.01, consistent with the experimental value (Figure 7C). It is possible that the protons generating this $^{D_2O}k_{cat}/K_{DHMP}$ are involved in the deprotonation of C2′−OH group and protonation of N5. Considering the pK_a of this group to be between 14 and 18 as expected for a secondary alcohol, the difference between the pK_a values of proton donor and proton acceptor would be significant, rendering this proton transfer considerably rate limiting.[26]

The proton inventory on $^{D_2O}k_{cat}$ revealed a much more pronounced dome-shaped profile, indicating that both normal and inverse solvent contributions were giving rise to the observed SKIE (Figure 7D). To properly interpret the results, nine different equations for distinct models describing proton inventories were compared (Table S2). Three of these models fit the data and are in agreement with the proposed chemical mechanism for this reaction (Scheme 2). The first is equivalent to the case discussed above for the $^{D_2O}k_{cat}/K_{DHMP}$ proton inventory, in which two transition-state protons with distinct normal and inverse fractionation factors are causing the SKIE. The second possible scenario predicts contributions from two transition-state protons with distinct fractionation factors accompanied by multiple inverse solvent contributions. Last, it is possible that two distinct transition states, contributing

dx.doi.org/10.1021/ja308350f | J. Am. Chem. Soc. 2012, 134, 19758−19771

with two protons each, are responsible for the dome-shaped proton inventory. According to Scheme 2, base abstraction of the C2′−OH proton and protonation of N5 occur through transition state 1 (TS1), to form I1. Next, π electrons from the C6═C1′ double bond abstract a proton from the conjugated acid of the base, and N5 is deprotonated, passing through transition state 2 (TS2) and forming HP. These two distinct transition-state models require the weighting factor to estimate the relative contributions of TS1 and TS2 to the observed KIE. The weighting factor revealed that one of the transition states is contributing for the majority of the effect observed (approximately 95% of the SKIE), and this illustrates why these three models fit equally well to the data. Despite the fact that the occurrence of two distinct transition states is likely, better fits and smaller errors were obtained when fitting data to a single transition-state model, which possesses fewer unknowns. The fractionation factors obtained for k_{cat} are $\phi_1 = 1.88 \pm 0.09$, $\phi_2 = 0.33 \pm 0.03$ (two distinct transition-state protons), $\phi_1 = 0.49 \pm 0.27$, $\phi_2 = 2.5 \pm 0.7$, and $\phi_{solv} = 0.52 \pm 0.40$ (two distinct transition-state protons, and a solvent contribution), both contributing to a calculated SKIE equal within experimental error to the experimentally determined SKIE value of 1.6. Previous work conducted on the dihydrofolate reductase from *M. tuberculosis* suggested that the N5 of 7,8-dihydrofolic acid has an inverse fractionation factor, and because both dihydrofolate and DHMP have identical pterin moieties, an analogous situation might be observed in the reaction studied here.[27]

It is important to point out that the first irreversible step in the reaction under steady-state conditions is glycolaldehyde release, so that the magnitude of the observed $^{D_2O}k_{cat}$ is diminished by subsequent events including HP release and other steps that increase the reverse commitment. Thus, because $^{D_2O}k_{cat}/K_{DHMP}$ includes steps up to and including glycolaldehyde release, reverse commitment factors are not decreasing its magnitude. This is corroborated by the presence of a burst of product formation (Figure 4), indicating that steps after the chemical step are limiting enzyme turnover (see upper portion of Scheme 6 for a comparison of steps that contribute to k_{cat} and k_{cat}/K_M).

It is difficult, if not impossible, to rule out media contributions to the SKIEs and proton inventory experiments conducted here. Similar proton inventories were observed in the reactions catalyzed by the aryl acylamidase from *Pseudomonas fluorescens* and tryptophan indole-lyase from *E. coli* in which media contributions arising from conformational changes and high commitment factors were associated with dome-shaped proton inventories.[28,29] Therefore, it is possible that the more pronounced deviation from linearity of the $^{D}k_{cat}$ proton inventory is due to increased commitment factors that are absent from $^{D}k_{cat}/K_M$. To summarize, the SKIEs discussed here clearly indicate the presence of offsetting normal and inverse contributions to the SKIE, and data are consistent with at least two transition-state protons with opposite contributions and possibly a solvent contribution to k_{cat}.

Single Turnover Experiments for the Aldolase Reaction. To obtain more information about the rate of chemistry in the aldolase reaction, the increase in fluorescence due to HP formation was monitored under single turnover conditions using limiting concentrations of DHNP or DHMP and increasing concentrations of *Mt*DHNA. Three exponential phases with opposite amplitudes showing no dependence on *Mt*DHNA concentration were observed when either epimer

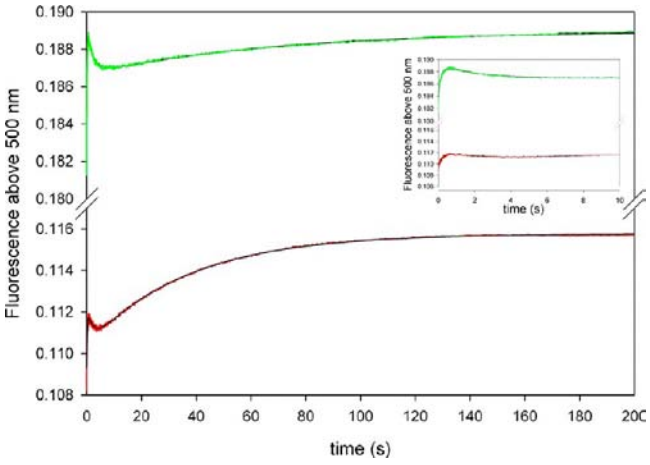

Figure 8. SKIEs under single turnover conditions. Data collected with 0.5 μM DHMP and 5 μM *Mt*DHNA. The lines represent fits to eq 3. The values obtained for k_2 in H_2O were divided by the ones obtained at 90% fraction of D_2O. The inset shows the first 10 s of the reaction, showing a clear increase in fluorescence followed by a slower decrease in fluorescence.

was the substrate (Figure 8). The first transient was characterized by a fast increase in fluorescence ($k_{obs1\text{-}DHNP}$ = 30 s^{-1}, $k_{obs1\text{-}DHMP}$ = 6 s^{-1}); the second transient showed decrease in fluorescence emission ($k_{obs2\text{-}DHNP}$ = 0.5 s^{-1}, $k_{obs2\text{-}DHMP}$ = 0.4 s^{-1}); and the third exponential phase was characterized by a pronounced slow increase in fluorescence ($k_{obs3\text{-}DHNP}$ = 0.019 s^{-1}, $k_{obs3\text{-}DHMP}$ = 0.025 s^{-1}). The third transient most likely represents HP formation, since it has rates comparable to the ones obtained in burst experiments ($k_{burst\text{-}DHNP}$ = 0.037 s^{-1}), demonstrating consistency as the burst rate must be larger than rates obtained under single turnover conditions since it can be extrapolated to the sum of the chemical steps in forward and reverse reactions and subsequent steps, such as product release.

To investigate what could give rise to the first two transients observed, simulations were conducted using Kintek Global explorer testing distinct mechanistic models that could generate the observed signals. Because the three phases observed showed no dependence on enzyme concentration, bimolecular steps were fixed at diffusion limit. A model testing whether formation of I1 could be giving rise to k_{obs1} was incapable of describing the experimental data, and very fast rates for formation and consumption of I1 were obtained. This is inconsistent with the SKIEs observed because it would suggest that chemistry was several orders of magnitude higher than k_{cat}, and if that was the case, SKIEs close to unity would be observed. The best-fitted model (bottom portion of Scheme 6) consisted of fast binding followed by an isomerization step causing an increase in fluorescence, after which this fluorescent species partitioned to form I1, and part of I1 was rapidly converted in DHXP. Both events (decay of the fluorescent species to form I1 and DHXP formation) caused decreases in fluorescence, after which protonation of I1 occurred causing an increase in fluorescence due to HP formation.

Dihydrobiopterin and other pterins have been shown to form oxidized quinonoid tautomers, which could possess a red-shifted maximum absorbance, if compared to nonquinonoid pterins, whose maxima is around 330 nm.[30,31] Therefore, it is possible that the first fast transient characterized by an increase in fluorescence represents a tautomerization step to form a

dx.doi.org/10.1021/ja308350f | J. Am. Chem. Soc. 2012, 134, 19758−19771

Scheme 5. Aldolase Reaction Is Shown in Blue, Epimerase Reaction in Green, and Oxygenase Reaction in Red, Including the Formation of the Proposed *para*-Quinonoid Species

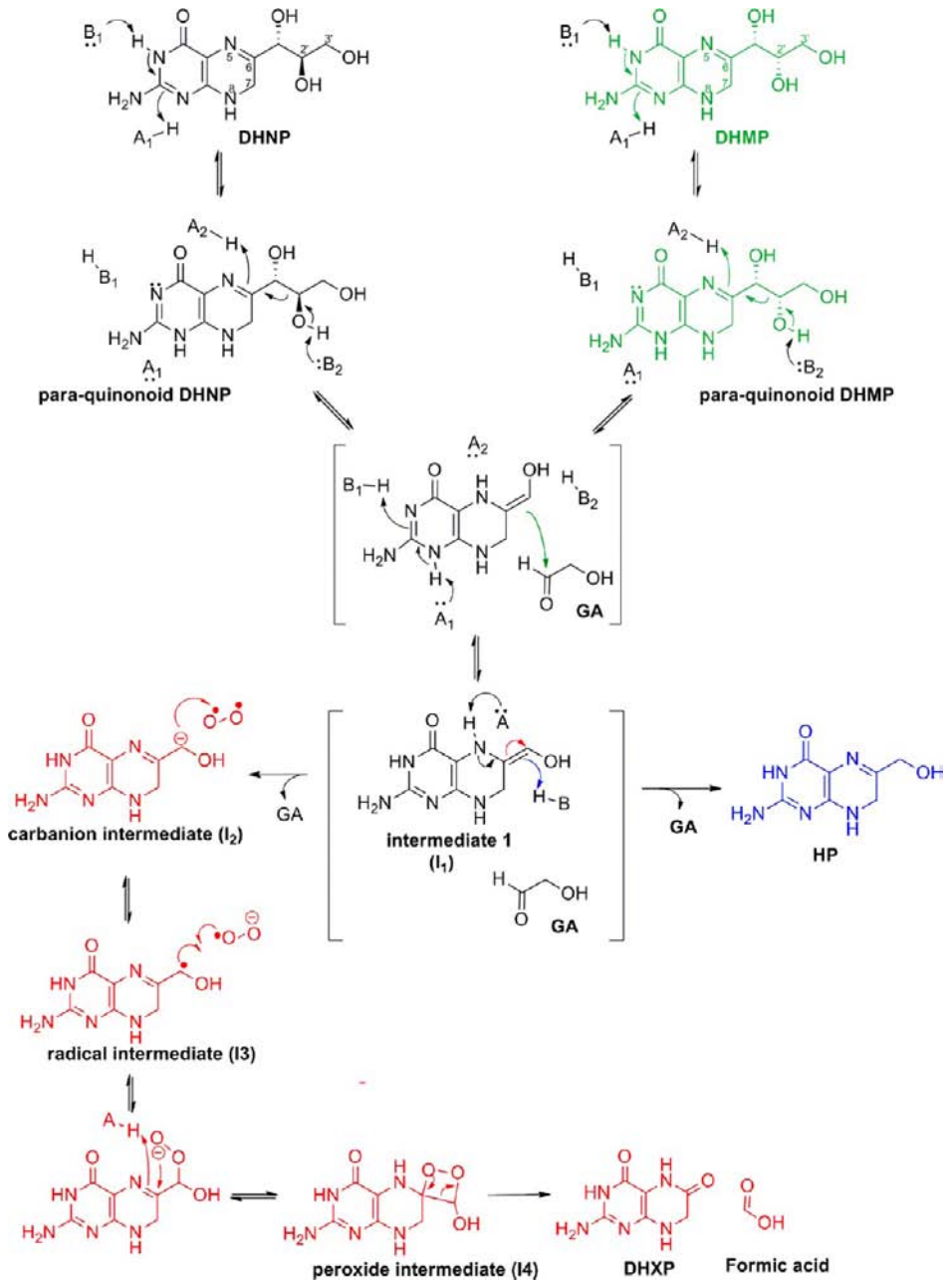

para-quinonoid form of DHNP. Scheme 5 shows an expansion of the chemical mechanism for this reaction, including the formation of the quinonoid species.

Pre-Steady-State SKIEs for the Aldolase Reaction. To better understand the role of rate-limiting proton transfers in the aldolase reaction, SKIEs were measured under single turnover conditions. DHMP was used as substrate due to the higher expression of KIEs as compared to DHNP. A limiting concentration of DHMP and increasing concentrations of *Mt*DHNA were utilized to ensure that experiments were conducted under pseudo-first-order conditions (0.5 and 2−5 μM, respectively). Three concentration-independent transients with identical appearance, as observed for single-turnover experiments conducted with DHNP as substrate, were observed both in H_2O and D_2O, indicating that only on-enzyme unimolecular steps were causing the changes in fluorescence. The first and fastest transient was characterized by an increase in fluorescence and an inverse solvent isotope effect of 0.6. As discussed above, the first transient is thought to be a tautomerization step, so that the observed effect is an equilibrium isotope effect instead of a kinetic effect.

The second transient was characterized by a decrease in fluorescence as a function of time, and no isotope effect was observed (KIE = 1.1). In contrast, the third slower transient corresponding to HP formation had a kinetic isotope effect (KIE) of 1.7. Interestingly, the amplitude of this transient in D_2O was 2-fold smaller than the amplitude of the same transient in the reaction measured in water. Because *Mt*DHNA catalyzes three distinct reactions, we hypothesized that the partition between each one of the reactions was no longer the

dx.doi.org/10.1021/ja308350f | J. Am. Chem. Soc. 2012, 134, 19758−19771

Scheme 6

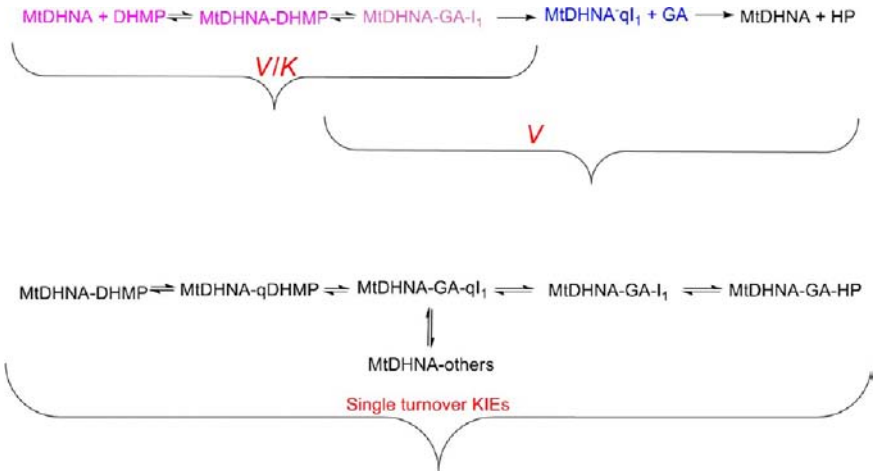

same when the reaction occurred in D_2O (*Mt*DHNA−DHNP or *Mt*DHNA−DHMP partitions in three distinct reactions in the first turnover, and 51% becomes the aldolase product, as discussed above). To test this hypothesis, *Mt*DHNA and DHMP were mixed at 10 and 3 μM, respectively, using standard reaction conditions in H_2O or 90% D_2O, the reaction was quenched after 200 s, and products were analyzed by HPLC. After separating DHMP and products, it was observed that the reaction in D_2O partitioned differently between the aldolase/epimerase/oxygenase reactions than the reaction occurring in water. In the reaction carried out in H_2O, the majority of product formed corresponds to HP, while in the D_2O reaction, less DHMP is consumed, less HP is formed, and more DHNP and DHXP are generated (Figure S10). We propose that the magnitude of the oxygenase reaction is related to the capability of the enzyme to protonate I1 to generate HP, so that any reduction in I1 protonation would allow this intermediate to react with molecular oxygen and form DHXP. It is likely that I1 protonation is slowed in D_2O, causing the aldolase reaction to occur less frequently.

Often, KIEs are measured under single-turnover conditions to decrease kinetic complexity since steps such as product release, which usually decrease the magnitude of observed KIEs by increasing reverse commitments, are not observed under these conditions. Nevertheless, the assumption that single turnover studies decrease kinetic complexity must be considered on a case-by-case basis. In the kinetic mechanism analyzed here, under steady-state conditions, release of glycolaldehyde is fast, causing the reverse chemical step to occur very rarely. Under single-turnover conditions, however, since only on-enzyme events contribute to the rates observed, the internal reversibility of the chemical reaction has a more significant contribution, therefore decreasing the magnitude of the KIEs observed under single-turnover conditions. Scheme 6 compares steps that contribute for KIEs under steady-state or single-turnover conditions.

Relevance of the Oxygenase Reaction. *Mt*DHNA is the first wild-type form of this class of enzymes to concurrently catalyze the epimerase and oxygenase reactions to a significant extent. Because the enzyme copurifies with bound DHXP, we conclude that the oxygenase reaction occurs *in vivo*, despite the fact that studies identifying and quantifying pterin molecules in *M. tuberculosis* are lacking. The fact that DHXP induces octamerization of the protein could have regulatory implications. It has been proposed that the substrate of the reaction, DHNP, is an antioxidant that could exert a protective effect on *M. tuberculosis* against host defenses, so that it would be advantageous for the bacteria to maintain the enzyme in the inactive *Mt*DHNA−DHXP form until enough DHNP was present to compete with DHXP and generate a productive *Mt*DHNA−DHNP complex.

■ ASSOCIATED CONTENT

Supporting Information

An extended description of proton inventory data fitting, ESI-MS spectra, and additional figures. This material is available free of charge via the Internet at http://pubs.acs.org.

■ AUTHOR INFORMATION

Corresponding Author

john.blanchard@einstein.yu.edu

Notes

The authors declare no competing financial interest.

■ ACKNOWLEDGMENTS

This work was supported by the NIH (AI33696), the Einstein-Montefiore CFAR (NIH AI-515109). We thank Dr. Bruce Palfey (University of Michigan) for help discussing tSKIEs and Dr. Richard Schowen (University of Kansas) for discussions about proton inventory data fitting. We also thank Dr. Luiz Pedro S. de Carvalho for critical reading of the manuscript and Dr. Rafael G. da Silva for insightful discussions.

■ REFERENCES

(1) Wright, D. L.; Anderson, A. C. *Expert Opin. Ther. Pat.* **2011**, *21*, 1293.
(2) Bermingham, A.; Derrick, J. P. *Bioessays* **2002**, *24*, 637.
(3) Walsh, C. *Nat. Rev. Microbiol.* **2003**, *1*, 65.
(4) Goulding, C. W.; Parseghian, A.; Sawaya, M. R.; Cascio, D.; Apostol, M. I.; Gennaro, M. L.; Eisenberg, D. *Protein Sci.* **2002**, *11*, 2887.
(5) Wang, Z. X.; Jiang, R. F. *FEBS Lett.* **1996**, *392*, 245.
(6) Sanders, W. J.; Nienaber, V. L.; Lerner, C. G.; McCall, J. O.; Merrick, S. M.; Swanson, S. J.; Harlan, J. E.; Stoll, V. S.; Stamper, G. F.; Betz, S. F.; Condroski, K. R.; Meadows, R. P.; Severin, J. M.; Walter, K. A.; Magdalinos, P.; Jakob, C. G.; Wagner, R.; Beutel, B. A. *J. Med. Chem.* **2004**, *47*, 1709.
(7) Johnson, K. A.; Simpson, Z. B.; Blom, T. *Anal. Biochem.* **2009**, *387*, 20.

(8) Johnson, K. A.; Simpson, Z. B.; Blom, T. *Anal. Biochem.* **2009**, *387*, 30.
(9) Wang, Y.; Li, Y.; Yan, H. *Biochemistry* **2006**, *45*, 15232.
(10) Bar-Even, A.; Noor, E.; Savir, Y.; Liebermeister, W.; Davidi, D.; Tawfik, D. S.; Milo, R. *Biochemistry* **2011**, *50*, 4402.
(11) Wang, Y.; Scherperel, G.; Roberts, K. D.; Jones, A. D.; Reid, G. E.; Yan, H. *J. Am. Chem. Soc.* **2006**, *128*, 13216.
(12) Wang, Y.; Li, Y.; Wu, Y.; Yan, H. *FEBS J.* **2007**, *274*, 2240.
(13) Fetzner, S.; Steiner, R. A. *Appl. Microbiol. Biotechnol.* **2010**, *86*, 791.
(14) Stein, R. A.; Wilkinson, J. C.; Guyer, C. A.; Staros, J. V. *Biochemistry* **2001**, *40*, 6142.
(15) Koshland, D. E., Jr. *Curr. Opin. Struct. Biol.* **1996**, *6*, 757.
(16) Goulding, C. W.; Apostol, M. I.; Sawaya, M. R.; Phillips, M.; Parseghian, A.; Eisenberg, D. *J. Mol. Biol.* **2005**, *349*, 61.
(17) Gieseg, S. P.; Amit, Z.; Yang, Y. T.; Shchepetkina, A.; Katouah, H. *Antioxid. Redox Signal.* **2010**, *13*, 1525.
(18) Firth, C. A.; Crone, E. M.; Flavall, E. A.; Roake, J. A.; Gieseg, S. P. *Biochim. Biophys. Acta* **2008**, *1783*, 1095.
(19) Duggan, S.; Rait, C.; Gebicki, J. M.; Gieseg, S. P. *Redox Rep.* **2001**, *6*, 188.
(20) Dantola, M. L.; Vignoni, M.; Capparelli, A. L.; Lorente, C.; Thomas, A. H. *Helv. Chim. Acta* **2008**, *91*, 411.
(21) Mathis, J. B.; Brown, G. M. *J. Biol. Chem.* **1970**, *245*, 3015.
(22) Harris, T. K.; Turner, G. J. *IUBMB Life* **2002**, *53*, 85.
(23) Highbarger, L. A.; Gerlt, J. A.; Kenyon, G. L. *Biochemistry* **1996**, *35*, 41.
(24) Abell, L. M.; Schloss, J. V. *Biochemistry* **1991**, *30*, 7883.
(25) Blaszczyk, J.; Li, Y.; Gan, J.; Yan, H.; Ji, X. *J. Mol. Biol.* **2007**, *368*, 161.
(26) Kyte, J. *Mechanism in Protein Chemistry*; Garland Publishing, Inc.: New York, 1995.
(27) Czekster, C. M.; Vandemeulebroucke, A.; Blanchard, J. S. *Biochemistry* **2010**, *50*, 367.
(28) Kiick, D. M. *J. Am. Chem. Soc.* **1991**, *113*, 8499.
(29) Stein, R. L. *Biochemistry* **2002**, *41*, 991.
(30) Lyudnikova, T. A.; Dashina, O. A.; Telegina, T. A.; Kritsky, M. S. *Appl. Biochem. Microbiol.* **2009**, *45*, 104.
(31) Eberlein, G.; Bruice, T. C.; Lazarus, R. A.; Henrie, R.; Benkovic, S. J. *J. Am. Chem. Soc.* **1984**, *106*, 7916.
(32) Skoog, D.; Holler, J.; Crouch, S. *Principles of Instrumental Analysis*, 6th ed.; Brooks Cole: Independence, KY, 2007.